Precipitating Cloud Analysis during Extreme Rain Events over the Chao Phraya River Basin Based on the Developed Radar Mosaic Products

Mahavik, N.[1] and Tantanee, S.[2]
[1]Department of Natural Resources and Environment, Faculty of Agriculture Natural Resources and Environment, Naresuan University, Phitsanulok, 65000, Thailand, Email: nattaponm@nu.ac.th
[2]Department of Civil Engineering, Faculty of Engineering, Naresuan University, Phitsanulok, 65000, Thailand

Abstract
During rainy season, Tropical Cyclones (TCs) regularly provide heavy rain over Indochina. In addition, the monsoon trough also produces rainfall to support agricultural activities across the area. However, the extreme rainfall events usually occur during the seasonal monsoon march. Understanding the precipitating cloud characteristics produced by the extreme rainfall events could alleviate the destruction of natural resources over Indochina. The variation in precipitating clouds can be analyzed using fine spatio-temporal resolution data, such as ground-based radar data from multiple radar stations. Since the Chao Phraya river basin is the most important basin in Thailand, this study is based on radar images collected from the five installed radar stations of the Thai Meteorological Department over this basin. The analysis of the extreme rain events during rainy season in 2018 was carried out using the developed mosaic method. Python and Open Source Computer Vision Library (OpenCV) were used in the development of mosaic products to focus on characteristics of precipitating clouds. Beam-blockage fraction was analyzed for each radar station and surrounding terrain using an open source library for processing weather radar data (wradlib) (Heistermann et al., 2013) with our developed beam-blockage analysis program. The severity of blocked beam is found over the northern mountain region of study area. The precipitating clouds were detected and their parameters extracted using the ellipse fitting technique. The analysis of these clouds revealed that, among other cases, Sontihn TC was a severely destructive event based on the storm parameters of both stratiform and convective clouds. The number and length of the convective storms during Sontihn TC was the most severe when compared to other events. It has been found that the diurnal cycle of the convective cloud shows their patterns by following solar heating surface over the study area for all of the selected events.

1. Introduction

Indochina is under the influence of Asian monsoon, where the agricultural activities of the area rely on rainfall. In addition, rainfall variations from Tropical Cyclones (TCs) can have many destructive impacts on human activities across Indochina. However, the inland devastation caused by TCs is due to strong winds and storm surge, which together cause loss of many lives. TCs normally undergo exponential decrease in intensity owing to the loss of kinetic energy or vorticity caused by the viscosity of the rough land surface and the shortage of water vapor over the land (i.e., Kaplan and DeMaria, 2001 and Roy Bhowmil et al., 2005). In Indochina, the total rainfall amount results from the contribution of westward-propagating TCs, typhoons, tropical storms, tropical depressions, westward-moving intraseasonal disturbances, and residual lows. TCs activity peaks in September, when it is estimated that 70% of the rainfall associated with TCs over Indochina occur (Takahashi and Yasunari, 2008). The Monsoon trough is also an important factor in modulating more westward-propagating TCs by producing above-normal precipitation over Indochina; it was a major factor in causing the 2011 flood in Thailand (Takahashi et al., 2015). However, the variation of TCs characteristics in term of precipitating clouds in both of stratiform and convective clouds are not well described over Indochina due to a lack of spatio-temporal observation data, such as ground-based radar products.

Both convective and stratiform precipitation coupled with TCs cause a longer duration of rainfall, which can increase the chances of flooding and loss of lives will occur (Jorgensen, 1984 and Yokoyama and Takayabu, 2008). It has also been found that convective and large stratiform rain areas that combine in mature mesoscale convective

systems (MCSs) such as cloud clusters and squall lines (e.g., Houze, 1989) are similar to TCs. However, the level of damage caused by TCs in Indochina depends on the velocity of TCs in the every decaying stage. Some TCs weaken much more slowly than normal storms after landing and they produce heavy rainfall, floods and landslides in the inland regions of Indochina (Sugimoto and Satomura, 2010). The frequent precipitation events that occurred during the rainy season of 2011 Thailand flood were clearly affected by the frequent westward-propagating precipitation systems toward Indochina (Takahashi et al., 2015). The flood was not caused by an atypical atmospheric circulation pattern based on statistical analysis of atmospheric circulation. However, a comprehensive comparative study of precipitating cloud characteristics in Indochina during the decaying stage of TCs has not yet been carried out.

Ground-based radar reflectivity provides information that is important in identifying the storm characteristics produced by TCs by revealing the spatial variability existing in the rainfall produced by TCs. Heavy rainfall can occur either hundreds kilometers from, or close to, the center of circulation on both sides of the storm track. For example, high rainfall occurred near the circulation center on the left side of Hurricane Danny in 1997 due to a slow forward velocity, a contraction of the eyewall and anomalously warm waters in Mobile Bay (Blackwell, 2000 and Medlin et al., 2007). Using radar reflectivity, Matyas (2010) found the relationships between the extent of a hurricane rain field, storm size and the environment surrounding the storm. The rainfall field data obtained from radar reflectivity has shown strong correlation with strong vertical wind shear in higher humidity. However, ground-based radar reflectivity products have not yet been disseminated to researchers in Indochina.

To understand storm morphology, the ellipse-fitting technique can be used on both radar reflectivity and Tropical Rain Mapping Mission (TRMM) Precipitation Radar (PR) or TRMM PR to find the major and minor axes length of the geometry extracted from geometry of the ellipses (Nesbitt et al., 2006 and Lang et al., 2007). In addition, Mahavik and Tantanee (2018a) applied the same ellipse fitting method to understand storm characteristics produced by Sonca TC based on the radar reflectivity observed by Phitsanulok radar, located in the middle of Thailand. Based on the estimation from radar reflectivity, the number of convective clouds extracted from the storm increased more than one time compared to the period of prior storm influence. However, the reported results were based on limited information from a single radar station; the components of both stratiform and convective clouds would not be well captured due to limitation of radar observation range. Consequently, it is expected that the mosaic products similar to Satomura et al., (2013) could bring more informative results on comparative storms in order to reveal the characteristics of storms produced by decaying TCs over the middle of Indochina.

This study is therefore motivated to produce comparative mosaic ground-radar reflectivity products of four selected rainfall events based on extreme precipitation influenced by decaying TCs and the monsoon trough. The study area is the Chao Phraya river basin in the middle of Thailand, and surrounding area covered by ground-based radar observation range. The mosaicked products are used in the extraction of storm characteristics and analyzed as comparative storm cases to address the severity of each selected storm.

2. Data and Method

2.1 Data and Study Area

In Indochina, there are two subseasons divided by the climatological monsoon break in late June (Takahashi and Yasunari 2006). Typically, the southwesterly monsoon has a major influence on rainfall for the first half of the rainy season (from May to June), whereas rainfall in the second half of the season (from July to September) is caused by active TCs. It is estimated that 70% of precipitation in Thailand is produced by TCs that cause rainfall to peak in September (Matsumoto, 1997 and Takahashi and Yasunari 2006). The study area of the Chao Phraya river basin is located in the middle of Indochina, and consists of mountainous regions in the north and a flood plain area in the middle and south.

Radar reflectivity data has been extracted from a freely accessible website hosted by Hydro and Agro Informatics Institute (HAII), and observed by the Thai Meteorological Department (TMD). Although TMD operates radar observation at the frequency of four times per hour, the original data is not available due to TMD restrictions. HAII provides the radar images at the frequency of only one hour; the radar reflectivity data in this study have been extracted from radar images in an hourly time scale. The extraction process has been done using a Digital Image Processing (DIP) method. The reflectivity from radar images has been studied by focusing on the precipitation clouds rather than using the original data of radar.

Table 1: Basic information of 5 radar stations

Radar	1st Angle (°)	Latitude	Longitude	Height (MSL)
1. Chiangrai (CRI)	0.99°	19°57′41.919″N	99°52′53.845″E	387
2. Lamphun (LMP)	0.48°	18°33′59.652″N	99°2′20.38″E	301
3. Phitsanulok (PHK)	0.50°	16°46′31.311″N	100°13′4.756″E	45
4. Chainat (CHN)	0.50°	15°9′28.06″N	100°11′28.436″E	17
5. Suvarnabhumi (SVP)	0.70°	13°41′10.732″N	100°46′4.8″E	1

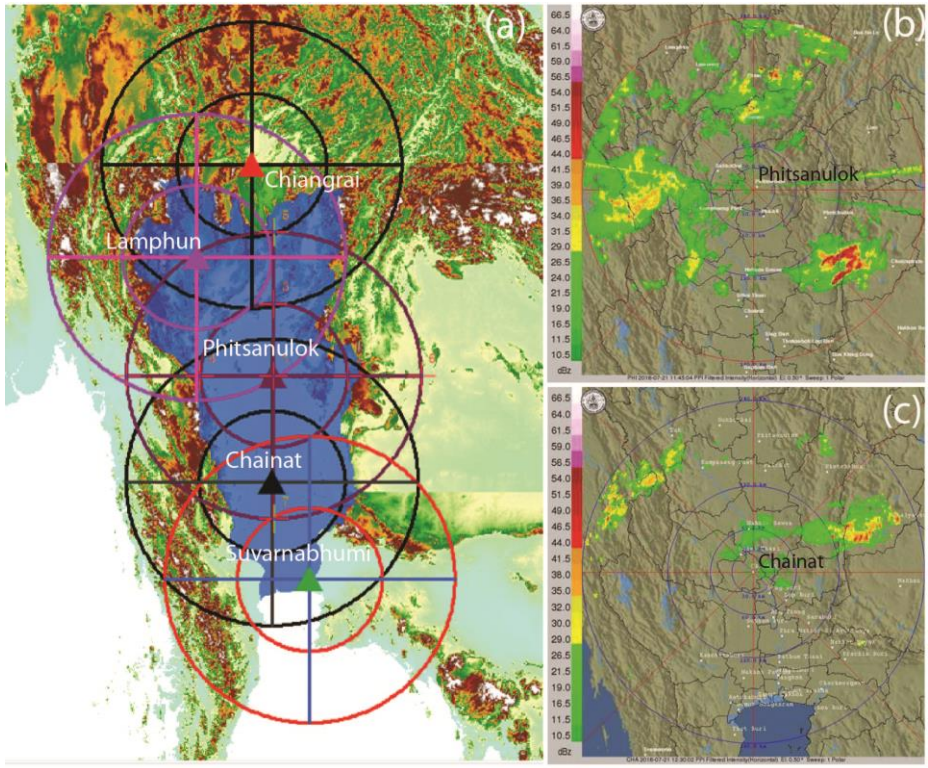

Figure 1: Study area and radar data used in the mosaic (a) Study area overlaid by observation area of each radar station shown in concentric circles, radar station shown in triangle, the Chao Phraya river basin shown in light blue region (b) Phitsanulok radar 2018112125 (c) Chainat radar 2018112130 for Sontihn

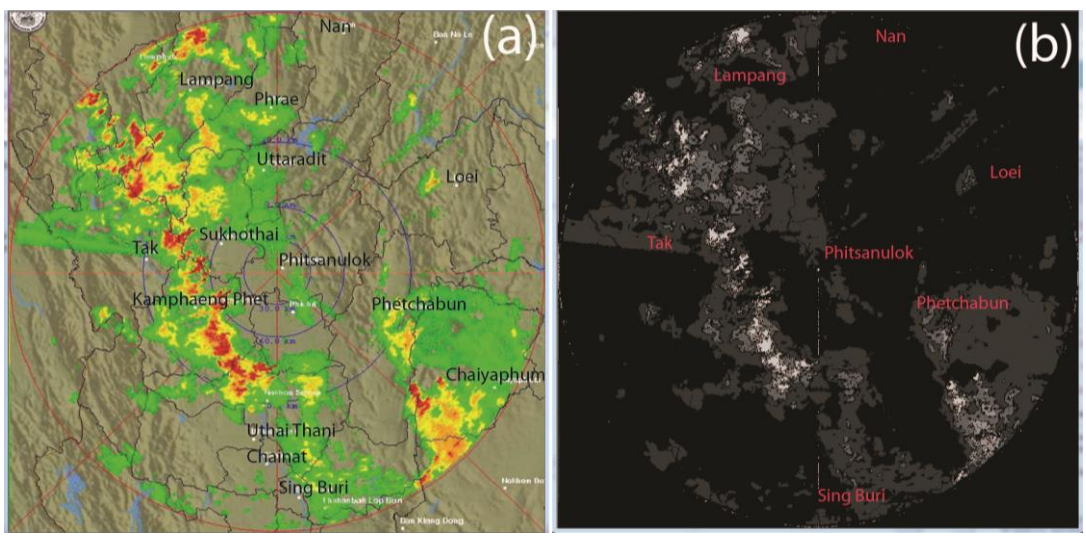

Figure 2: Radar reflectivity extraction (a) original radar image of Phitsanulok at 201707261125 (b) extracted radar reflectivity

Table 2: Basic information of extreme events

Event name	Period	No. of radar files
1. Monsoon trough (R1)	20180601-20180610	229
2. Sontihn (R2)	20180715-20180724	237
3. Bebinca (R3)	20180813-20180822	226
4. Barijat-Mangkut (R4)	20180910-20180921	252

Five stations covering the whole Chao Phraya basin, the most important basin for Thailand, and neighboring areas were selected for use in the reflectivity mosaicking (as shown in Figure 1). The basic specifications of these five radar stations are shown in Table 1. As can be seen in Figure 1, the radar range of 240 km of these 5 stations allows for coverage of the entire study area. All 5 stations operate in PPI mode of C-band frequency, described in the original radar images. The data that have been provided to public are the 1st PPI data. At present, TMD also provides the radar reflectivity composite product on their website. The elevation angle is adequate for scanning over the flat terrain in the central part of Thailand. However, the complex terrain located over the northern part of Thailand causes a problem in radar observation due to radar beams being blocked by surrounding terrain. Since the upper part of the study area is also located in this area, beam blockage analysis for each station was investigated with SRTM DEM V4 with resolution of 3 arc seconds (Rabus et al., 2003) to understand radar quality. DEM is prepared by merging all tiles over the study area, and then is clipped to fit for the radar coverage used in the analysis of beam blockage by terrain.

Due to the radar coverage over the middle and lower part of the study area, Phitsanulok and Suvarnabhumi radar stations are used to meet the minimum requirement in the mosaicking process. When data is missing for either Chiangrai or Lamphun radars, data from Phitsanulok radar can provide acceptable replacement information for the mosaicking processing. The mosaicking process cannot be carried out whenever Phitsanulok data is unavailable.

2.2 Extreme Event Cases

The studied rainfall events are based on TMD warnings issued in the 2018 summer monsoon Table 2. The first case was caused by the monsoon trough, and the other cases were caused by TCs. In order to capture the effect of the extreme events, the 3 offset dates in the selected cases were applied before and after the warning periods issued by TMD. The total number of radar images collected for the studied period comprises 964 files created on an hourly basis.

2.3 Tools

To process such a large amount of data, the python scripting language V.2.7 of the Anaconda V.3 package, as previously used by Mahavik and Tantanee (2018a), is utilized in this study. All radar pixels are stored in a NumPy array. Digital Image Processing in computer vision technique is used by employing Open Source Computer Vision Library (OpenCV) using Python script interface. Python is a very high level interpreted object oriented programming language with a rich set of data types. The advantage of using Python is that it is easy to learn as a powerful language that is freely available, widely used, and well supported on a variety of computers and operating systems. A Radar Echo Classifier algorithm was also developed in Python to identify various radar echoes such as precipitation, clear air, and, in particular, anomalously propagated (AP) ground clutter in NEXRAD radar data (Van Andel, 2001). OpenCV library was mainly used to develop algorithms in the radar mosaicking process. The Wradlib library (Heistermann et al., 2013), an open source library of weather radar developed by Python script, is used in our investigations of the mosaicking to analyze beam-blockage fraction from a simulated radar beam interacting with terrain of its propagation through standard atmosphere.

3. Methodology

3.1 Radar Extraction

Precipitating clouds, as the main important phenomenon in this study, are extracted from the radar images downloaded from HAII. The intensity of radar reflectivity is standardized by TMD using the same color schemes for all radar stations, ranging across green, yellow, orange, red and purple for light, moderate, strong, and heavy rain, respectively. During the extraction process, the reflectivity was converted to the same color scheme. All radar images must be converted JPEG picture format with 800x800 pixels of resolution. The area outside observed radar range is removed to prepare the data for the next step. Before conversion to grayscale range, the foreground data of the radar images is extracted using OpenCV by setting a color range for the returned radar reflectivity (as shown in Figure 2). This is done in order to be able to process the next step of morphological operation in the

quality control process, before the mosaicking process.

3.2 Radar Mosaic and Quality control

3.2.1Radar quality control

Radar quality control is assessed for each station to screen out the low quality radar images from the mosaicking and analysis processes, as shown by the workflow in Figure 3. The first control is to detect radar flares, which interfere with the beam signal during observation. Radar flares appear in the cone of the radar beam, but are not related to rain region, as shown in Figure 4. The second control is to detect and reject any radar image appearing to contain a relatively large bad strip that may be caused by image processing after receiving the radar signal.

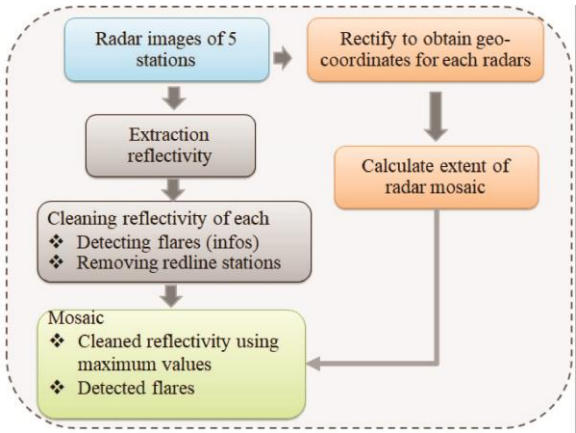

Figure 3: Workflow for radar mosaic

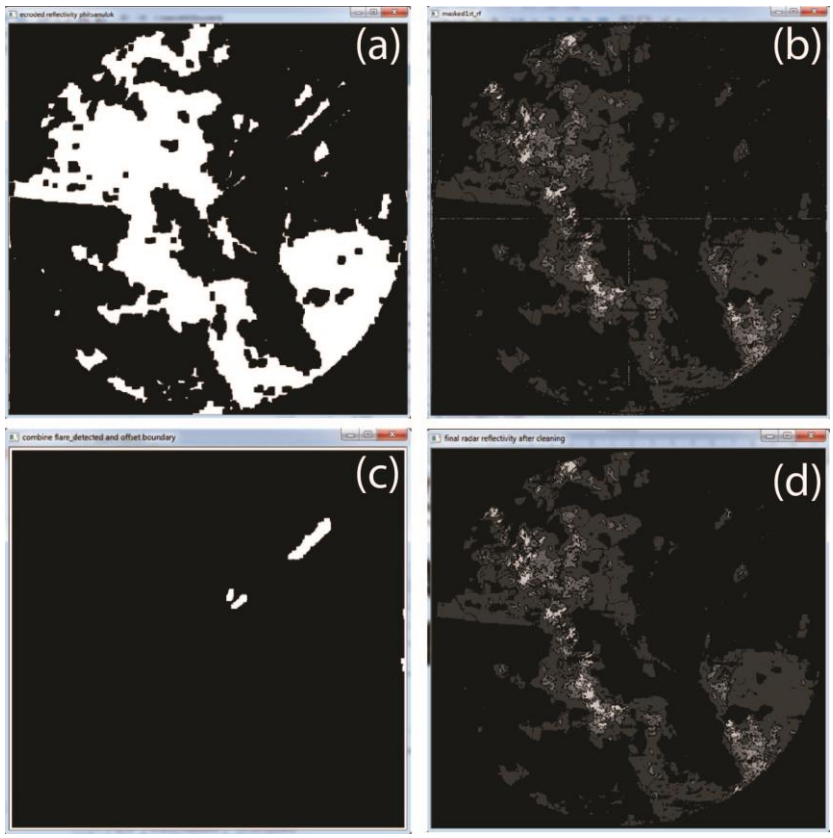

Figure 4: Processing of the extracted radar reflectivity (a) result of applying morphological eroded operation using kernel convolution at 9x9 window size (b) the extracted radar with flares and lines (c) detected flares and offset bound (d) final result after applying the Eroded 9x9 result as shown in Figure 4a to remove the detected flares and offset bound

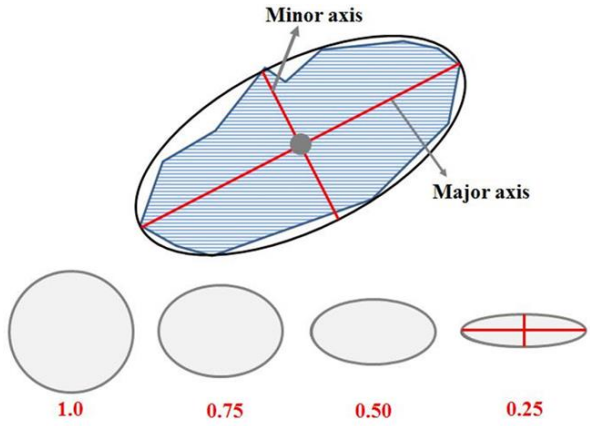

Figure 5: Schematic of the fitting ellipse shown in the biggest ellipse envelopes of the convective region in blue region. The axis ratio (AR), the ratio between minor and major fitting ellipse length, is shown as a number

Radar flares can appear in both permanent and non-permanent locations. To remove radar flares, morphological operations of open and close with eroded kernel are applied to the extracted reflectivity in grayscale color with the kernel convolution at the sizes of 7x7 and 3x3, respectively. By applying morphological operations, small holes in the extracted reflectivity, and the possible flare regions, can be traced using the contour function of OpenCV. The radar flare detection is carried out using an ellipse fitting in OpenCV from fitEllipse as also used in Mahavik and Tantanee (2018(a) and 2018(b)). Criteria of radar flare detection are defined through the ellipse fitting with the defined eccentricity less than 0.25. The geometry of the ellipse can be calculated from major and minor axes of the ellipse fitted to the contour region, as shown in Figure 5. The length of the major axis of the fitted ellipse is also applied at the minimum threshold of more than 20 km. The threshold value for both eccentricity and length of major axis from ellipse fitting are obtained by many trials to find appropriate threshold used in the detection.

To detect and reject a large bad strip, ellipse fitting is also used with a region of large size pixels applied at a threshold of 13,000 km^2. The detection process in Python will repeat until it can detect the defined criteria for both radar flares and bad strips. The program, then, will mark those regions of pixels, and will generate a report for each radar image file.

3.2.2 Beam propagation interacting with surrounding terrain

To reconstruct a propagating radar beam through the atmosphere, the spherical coordinated radar reflectivity is considered with the elevation above Mean Sea Level (MSL). MSL is obtained from the SRTM Digital Elevation Model (DEM) V4 with resolution of 3 arc seconds (Rabus et al., 2003) for range bin at a resolution of 1 km. The height of each range bin is calculated using the standard refraction relation from Rinehart (1999), as shown in equation (1):

$$H = \sqrt{r^2 + R'^2 + 2rR' \sin \emptyset} - R' + H_0$$

Equation 1

where H is the height of the range bin, r is the observation range from the radar to the point of interest, ø is the elevation angle of the radar beam, H_0 is the height of the radar antenna, which is approximately 30 meters plus the elevation of the radar station above mean sea level obtained from DEM, R' = 4/3R, and R is the earth's radius (approximately 6374 km).

3.2.3 Mosaic radar products

Since the radar image is not provided with the coordinates, georeferencing of the radar images is computed in the geographic coordinate system using GIS, before mosaicking radar reflectivity. All radar images are processed with the 1st order of polynomial functions. Therefore, the positions of all pixels from radar images are fixed to the coordinate system that will be used in the mosaicking tasks. Before mosaicking, the criteria of a number of studied radar stations for each observed time step must be satisfied. Due to data being unavailable for some scanning times, the developed mosaic algorithm must be sure that the mosaic output covers the study area. Due to the location of the radar stations, the first requirement for radar images is that images must be obtained, at least, from either Phitsanulok or Chainat station.

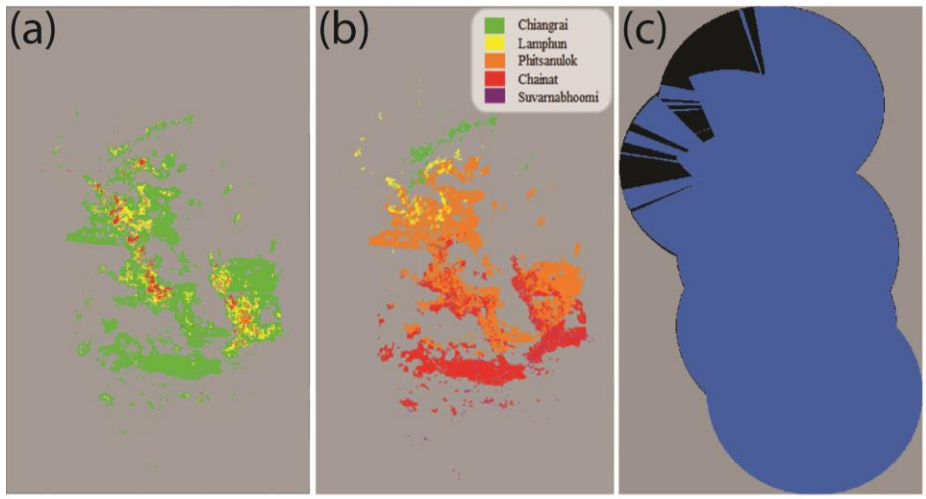

Figure 6: Radar mosiac products (a) radar reflectivity (b) used radar information for each pixel (b) beam blockage at 75% of beam width

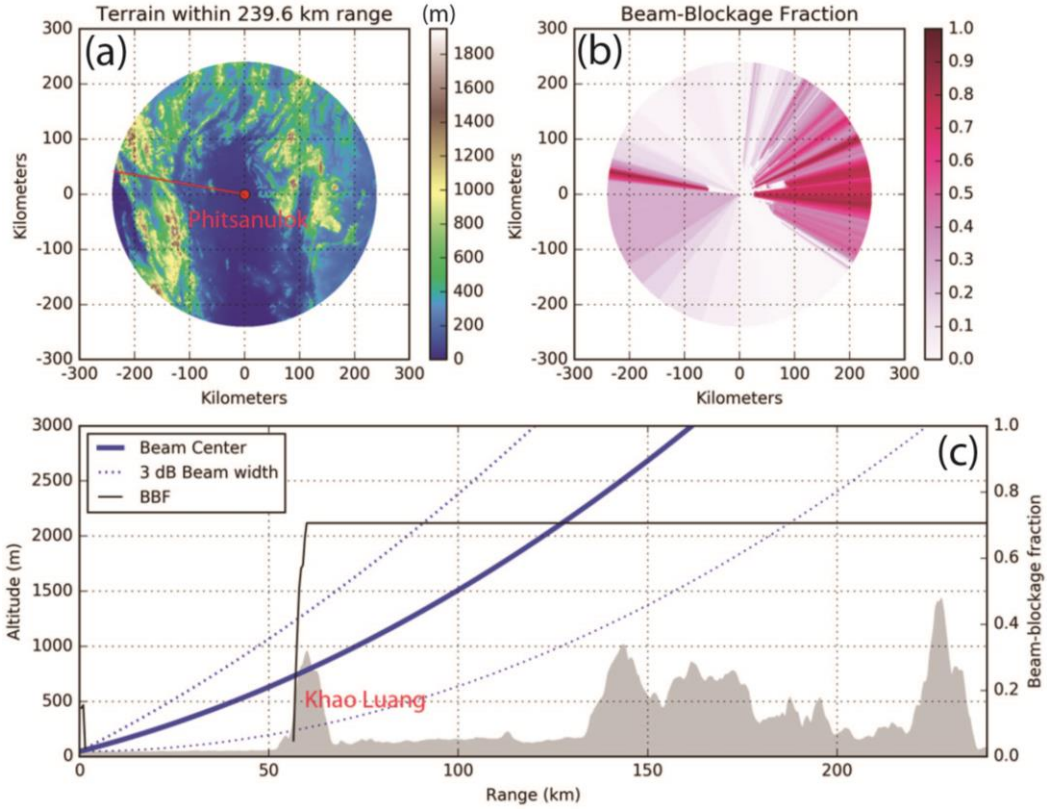

Figure 7: Beam-blockage fraction obtained from simulated radar beam for Phitsanulok radar (a) direction indicator in azimuth as shown in red line over terrain (b) beam-blockage fraction over the observation ranges (c) simulated beam propagating through standard atmosphere interacts with terrain at specific azimuth

The second criterion is that a minimum of at least three radar stations must be used. The mosaic output is rejected and the output is not used when any of these criteria are not met. The report of success and failure based on these defined criteria is produced and used in analysis of the mosaic output.The output array of the radar mosaic is defined at a resolution of 0.00695° based on the original radar image. The NumPy array used in Python script can store all of the radar pixels from the extracted reflectivity. In this step, the maximum value of the radar reflectivity, as identified by TMD color scheme, is used as a criterion where the output pixel has more than one value of reflectivity due to overlapping

regions of radar observations. Finally, the mosaic output for each scanning time is produced as a radar mosaic product of precipitating cloud (as shown in Figure 6a). Each mosaic pixel output is produced and incorporates the mosaic product of precipitating cloud based on the radar reflectivity (as shown in Figure 6b). In addition, the mosaic output of radar flares is also produced from scan to scan times. The effective area of defined percentage of beam blockage by terrain is also produced in the mosaic product in order to understand the coverage area, which depends on quality of radar observation (as shown in Figure 6c). The obtained mosaic products will be used in the analysis of comparative extreme rain events in the next session.

3.3 Precipitating Cloud Detection and Extraction

Focusing on precipitating cloud of the extreme events, the radar mosaic output of each hourly observation is used to extract data on the precipitating clouds. The comparative study of clouds in each event is investigated for both in-total comparison and diurnal cycle of clouds based on reflectivity. The convective cloud data is derived by applying the convective cloud extraction. The detection and extraction data of convective clouds is analyzed under the concept of the ellipse fitting by employing the geometry of the fitted ellipse. To separate convective and stratiform clouds, the convective cloud is defined by a color scheme that indicates moderate rain to heavy rain. Therefore, the convective cloud and stratiform cloud regions are delineated using the defined criteria. However, to further detect the convective regions, the criteria based on the fitted ellipse must be defined using three conditions. The first condition is that the detected convective region must have a major axis of the fitted ellipse in the range of 5 to 1,000 km. The second condition is that the detected convective cloud must have eccentricity larger than 0.1 to assure that the shape of the cloud region is not too elongated. The last condition is to assure that the convective cloud area is not too small by applying the fitted rectangle as a function of OpenCV by setting the minimum of area at 10 km^2. The extraction of convective cloud has been computed through the whole area of each mosaic output to find those convective regions that satisfy the criteria

4. Results and Discussion

4.1 Beam Blockage Analysis

Radar stations operated by TMD are mostly located in urban areas, for the purpose of providing weather information over urban area where people are living. Radar observation can also provide near real-time weather information to aviation traffic over an airport. The radar stations in this study are located at the meteorological observation offices, except for the Phitsanulok radar station. The radar beams are often affected by surrounding terrain in the mountainous regions, especially when 1st elevation angle of the radar observation is used. The simulated radar beam for the 1st elevation of both Chiangrai and Lamphun stations is affected, with a high percentage of beam blockage by terrain analyzed with DEM. The western part of the radar observation area at Chiangrai radar shows a blind observation radar area on higher beam-blockage fraction visualized in Wradlib compared to the eastern side.

However, the other three radar stations, which are Phitsanulok, Chainat and Suvarnabhumi, are quite clear from terrain blockage of observation beams due to the relatively flat area of the Chao Phraya basin. As shown in Figure 7, the western part and some beam range of eastern part of Phitsaulok radar show simulated beam blockage by terrain. When comparing the mosaic area of simulated radar beam observation for each threshold, at 50% and 75% of beam blocked by terrain, effective observation beams that indicate usefulness over large portions of the study area were demonstrated. Although the radar observation of TMD operates in four elevation angles, the raw radar data is not accessible for Thai researchers. Therefore, this study was done by using only 1st elevation angle of radar observation. If possible, future work should be done by using multiple elevation angles of raw radar data in the mosaicking process in order to avoid the beam blockage problem. Study of this type would require raw data similar to the study by Fulton et al. (1998) that used in an operation of the Next Generation Weather Radar (NEXRAD) program using Weather Surveillance Radar-1988 Doppler (WSR-88D) radars across the United States.

Beam blockage analysis is very useful for setting the radar scanning strategies for a particular site. Surrounding terrain plays an important role in the proper interpretation of reflectivity data for understanding the extent to which a radar view is blocked by obstacles. In the present study, the results are based on the assumption of the simulated propagating beam through standard refraction of atmosphere interacting with DEM which is extracted from SRTM. Kucera et al., (2004) used Geographic information systems (GISs) combined with digital elevation models (DEMs) to assess the radar beam blockage and other ground clutter phenomena using radar reflectivity for the U.S. Air Force Weather Surveillance Radar-1988 Doppler (WSR-88D) in Guam. Even though higher

resolution of DEM provides better results, lower-resolution DEM is more widely available. Recently, McRoberts and Nielsen-Gammon (2017) used long-term precipitation climatology data with no prerequisite knowledge of topography to identify the blockage area of the radar beam by topography in gridded radar-based quantitative precipitation estimates (QPEs).

4.2 Radar Mosaic Products and Precipitating Cloud Extraction

The radar mosaic products are produced based on the developed algorithm to focus on precipitating cloud characteristics in comparison of extreme rainfall events. The quality of radar reflectivity data is the key factor needed to assure the quality of analysis. In this study, 964 files comprised the total radar data used for all selected rainfall events, with the number of radar reflectivity files used varying with each rainfall event period; however, the differences were not large, as can be seen in Figure 8. In addition, missing and low quality data based on criteria as mentioned above causes further differences. There was a large amount of missing and low quality data during the events of Bebinca and Barijat-Mangkut storms. The missing number of files for each rain event demonstrates the technical operational problems faced during observation of TMD. In order to avoid this problem, it is suggested that TMD should archive and freely publish all of the observed radar data for both radar images and raw radar data, with some restriction rules imposed on researchers so that analysis of extreme rainfall events can be done more accurately in order to contribute to scientific knowledge from research to society.

In developed countries, the radar mosaic products have operationally used for weather forecasting and hydrological monitoring. The Next Generation Weather Radar (NEXRAD) Precipitation Processing System (PPS; Fulton et al., 1998) have been implemented and used in weather operations in U.S. for many years. Moreover, the National Mosaic and Multi-sensor Quantitative Precipitation Estimation (QPE) System (NMQ; Seo et al., 2005, Vasiloff et al., 2007, Langston et al. 2007 and Zhang et al., 2005, 2011), which is the latest product of a joint effort among several NOAA and non-NOAA offices, has already been used for hydrology and water resource applications. By contrast, in developing countries, including Thailand, the radar systems are not yet unified on both radar instruments and systems, although the coverage of radar observation over Thailand is extensive. The present work should be seen as an initial step toward implementation of a sophisticated radar mosaic system based on 3 dimensional radar data for Thailand, similar to the work of Zhang et al., (2005, 2011). Zhang et al., (2005) carried out investigations in the U.S to find an analytical approach to construction of a 3D multi-radar mosaic scheme in a Cartesian framework from Spherical coordinates of raw data. The volume scans of multiple radars were used during horizontal and vertical interpolations to retain high-resolution structures comparable to the raw data. Mahavik et al., (2014) have used the raw data of volume radar scans to create a constant altitude plan position indicator (CAPPI) at 3 km. The radar product can be used in validation of the simulated results from a mesoscale numerical model to compare the storm structures (Satomura et al., 2013). Using multiple elevation angles, one can manage to provide appropriate weighting from defining effective radius of radar bin to considering output grid. However, the radar mosaic output and the developed mosaic method will be useful to TMD for real-time monitoring of severe precipitating cloud forcing by severe weather. In the present study, the raw data of volume radar scans is not accessible from the TMD database. The raw radar data were used in analysis of radar rainfall estimates and rainfall pattern in the middle in Indochina similar to works by Mahavik et al., (2013 and 2014) and Mahavik and Tantanee (2019). Therefore, the precipitating cloud classification method simply relies on color ranges of the radar reflectivity in this study. The radar instrument calibration is a key process to insure standardized radar reflectivity product that may have slightly different settings among the five stations, and the quality of the obtained simple classification of precipitating convective clouds highly depends on those calibrations. Using the complex and multiple parameters of retrieved radar moments, a fuzzy logic algorithm is used to classify radar echoes for Weather Surveillance Radar-Doppler 1988 (WSR-88D) (Kessinger et al., 2003). The intensity and sharpness of the peaks of echo intensity extracted from raw radar reflectivity are used to easily separate convective and stratiform regions (Steiner et al., 1995).

4.3 Storm Characteristics on Extreme Rainfall Events

Using multiple sources of radar information can provide direct advantages for the re-analysis of precipitating clouds over a large basin during extreme rainfall events. The results of comparative storm information extracted from the mosaic radar products have shown qualitative information during the seasonal monsoon march of the boreal summer over the Chao Phraya river basin in 2018.

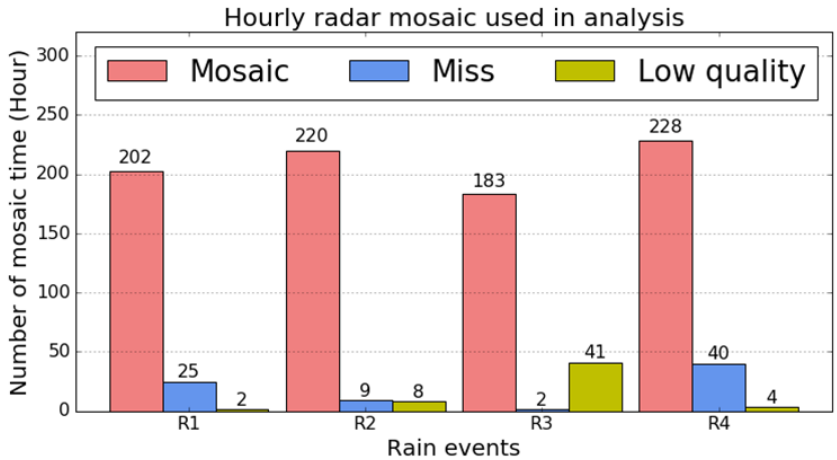

Figure 8: Comparative statistics of all radar mosaic output for all rain events describing the completeness and quality of data used for the radar mosaic processing

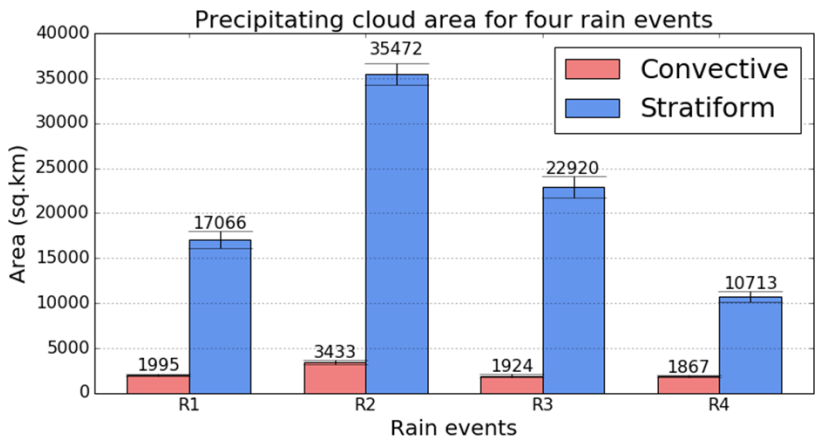

Figure 9: Comparison of precipitating clouds for both stratiform and convective regions in all rain events

4.3.1Characteristics of storm events

The qualitative comparison between stratiform and convective clouds of the four selected events is shown in Figure 9. Not surprisingly, precipitating cloud associated during the decaying stage of Sontihn TC (R2) over the middle of Indochina shows the large area and large number of storms. However, the producing convective area in the beginning rainy season (R1) during strong monsoon trough shown to have been relatively large in both area and number of storms as compared to other rain events. The hourly average results of the extracted storm characteristics, which are area, number and length of the convective storm, as shown in Figure 10, expresses the severity of the selected rainfall events. When comparing the hourly average of the other convective storm rain events, the most severe is shown to be. The severity of convective storms on the R1 monsoon trough also needs to be addressed since the storm has shown a high variation of the storm numbers, as shown in Figure 10, compared to R2. Further investigation of classifying characteristics such as area and length of the storm (as shown in Figure 11) can provide more information of convective storm severity. Sonthin(R2) is found to be the largest storm measured by these characteristics. Based on precipitation gauge data and long-term satellite precipitation data, it is found that the frequency of extreme rainfall over some areas, including the Indochina region, has increased in the last several decades (Karl and Knight, 1998, Groisman et al., 2004 and Lau and Wu, 2007). Over the northwest Pacific, where Indochina is located, there has been a reduction in TCs rain that may possibly be associated with a strong interdecadal-scale oscillation (Lau and Zhou, 2012). In addition, decreased frequency in heavy-rain storms and

increased frequency in light-rain storms have been found over the northwest Pacific portion. The studies on rainfall related to TCs over Indochina have shown that rainfall during the month of October, which is the monsoon retreat period, has increased in the last 40 years over and around northern Vietnam. These increases are associated with the long-term changes in TCs (Takahashi, 2011). The long-term decrease in rainfall over the Indochina Peninsula has been most significant along the eastern coast of Vietnam, where rainfall is strongly affected by TCs. However, Kanae et al., (2001) found decreased rainfall in September over Indochina in the second half of the twentieth century. Takahashi and Yasunari (2008) and Takahashi et al., (2009) proposed that the long-term decrease in rainfall over Indochina in September could be explained by the weakening of TC activity over the South China Sea and Philippine Sea regions. In this study, even though the four selected extreme rain events were analyzed, the results cover a time frame that is relatively too short for explanation of precipitating cloud changes. Study of the longer-term data from extreme events is needed to reveal the precipitating cloud changes over the basin.

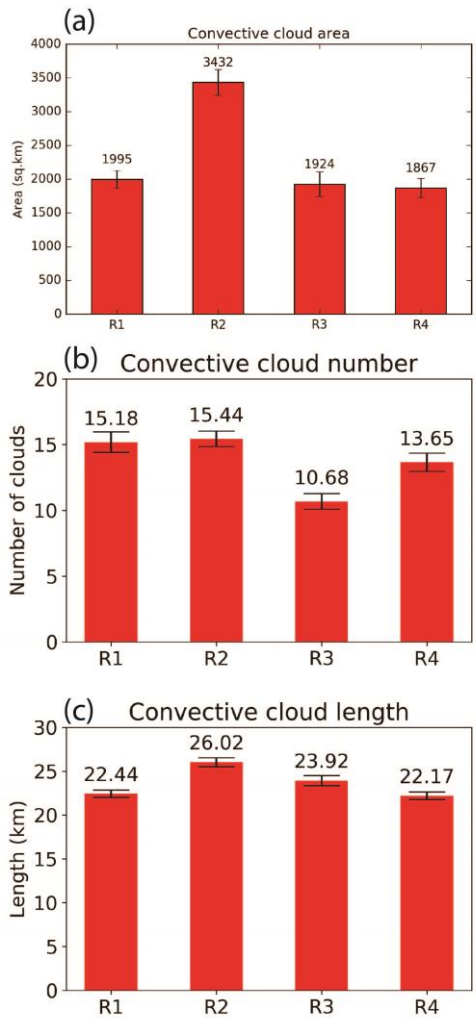

Figure 10: Hourly averages of the convective clouds for all of the rain events (a) cloud area (b) cloud number (c) cloud length

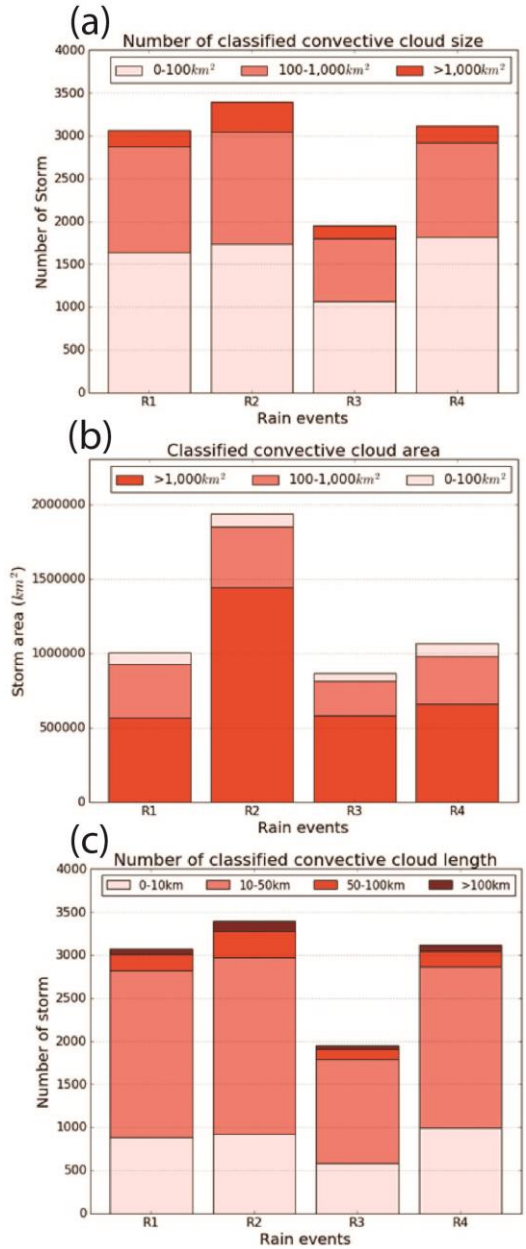

Figure 11: Classified convective clouds for all events (a) number of convective cloud classified by cloud area (b) cloud area (c) cloud length

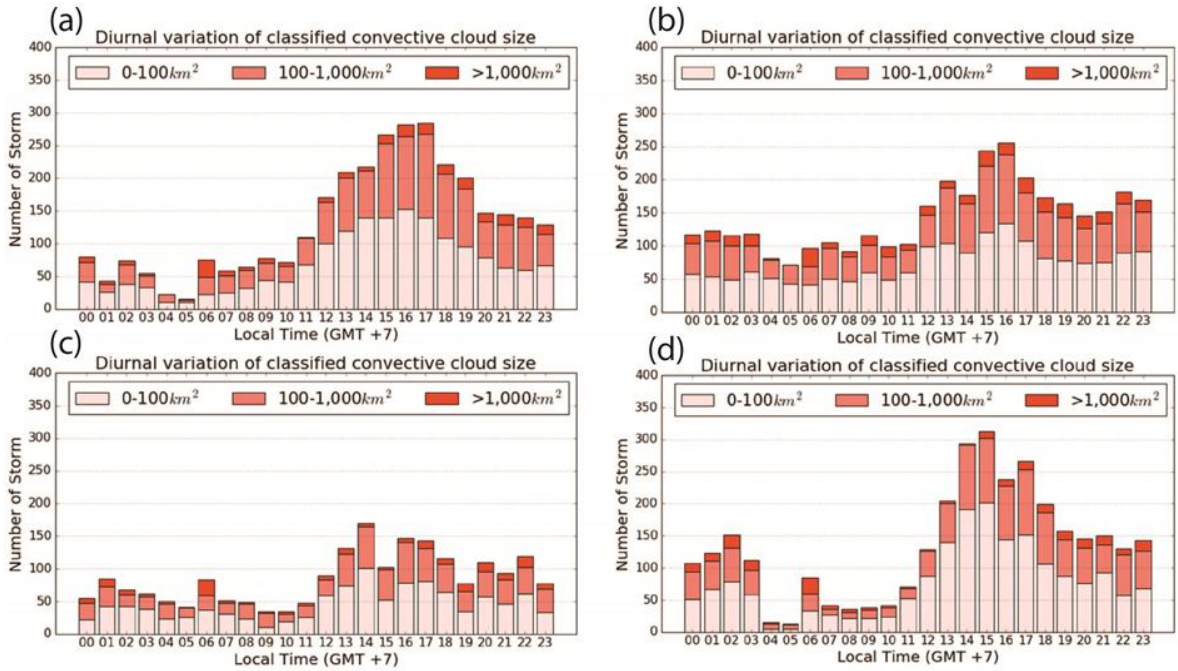

Figure 12: Diurnal cycle of the convective storm number for each rain event by classified convective regions (a) R1 (b) R2 (c)R3 (d)R4

4.3.2 Diurnal cycle of storm characteristics

Patterns of convective storm characteristics are further investigated to analyze variations in storm severity during the day. The distinguished diurnal cycle pattern between convective systems produced by TCs and the monsoon trough is recognized by the classification of storm number, as shown in Figure 12 and storm length (Figure not shown). The diurnal cycle of storm area size is clearly shown to peak during the monsoon trough event (R1) compared to convective storms produced by TC events. However, precipitating convective cloud shows the same pattern as the diurnal cycle of surface heating, although the peaks of the diurnal cycle of convective cloud vary from rain events respective to local time.

In the mid-latitudes, the growth of rain field size was studied by using radar reflectivity during the decaying stage of TCs landfall in U.S. (Matyas, 2013). The diurnal cycle influences rain-field growth during the late morning and early afternoon, which is between the times for peak area extent of oceanic- and land-based precipitation in the tropics. A shift in the rain-field peak from before midnight during the years 1950–96 to after midnight during the years 1995–2008 was found. In the present study, in the case of TC landfall over the tropical area, the peak of convective storm numbers occurs from the late afternoon to evening. In addition, narrow mountain ranges comprise an important organizing agent anchoring monsoon convection centers on the windward side (Xie et al., 2006). Using TRMM PR, it has been demonstrated that the Mesoscale Mountains of Asia are an important agent for organizing monsoon convection through a strong interaction between convection and circulation. Additionally, topography plays a significant role on the rainfall pattern over the Indochina. The phase delays of radar echoes deepened on the leeward side of prevailing wind for both winter and summer monsoon over the western part of Indochina. In the present study, the diurnal cycle of convective cloud is mixed for both southerly monsoon and TCs forcing that come from southwesterly and easterly prevailing winds. The evening peak identified in our convective cloud analysis is consistent with the radar echo peak of Okumura et al., (2003). However, our analysis does not agree with Satomura et al., (2011), who found that the radar echo peak over Vientiane radar observation in the eastern part of Indochina occurred at 0100 local time in July of 2008.

5. Conclusion

The free access of ground-based weather radar images operated by Thai Meteorological

Department (TMD) were used to analyze precipitating clouds produced by extreme rainfall events during the 2018 rainy season over the middle of Indochina, where the study area of the Chao Phraya river basin is located. Hydro and Agro Informatics Institute (HAII) provided the radar images of the first elevation angle at the frequency of once per hour, and these were used to develop the radar mosaic products with five radar stations covering the whole basin. Using python, Open Source Computer Vision Library (OpenCV) and an open source library for processing weather radar data (wradlib) (Heistermann et al., 2013), the radar mosaic product of precipitating clouds was created using the developed method to focus on the characteristics of both stratiform and convective clouds. Quality control is a critical element of radar mosaic creation with regard to both minimum requirements of radar stations and the quality of collected information, itself.

The ellipse fitting technique was used to detect radar flares, and was also used to extract the convective storms inside the radar mosaic product. By considering the terrain from Digital Elevation Model of SRTM, the beam-blockage fraction informs the quality of radar observation for recognizing the severity of radar observation over the mountainous region of the northern part of the study area. In performing the analysis of precipitating cloud detection and extraction, the cloud characteristics produced during the four extreme events were compared. The severe Sontihn TC shows the largest measured parameters on convective clouds for number, area and length. The diurnal cycle of the convective clouds shows their patterns follow solar heating of the surface over the tropical area for all selected events. However, the diurnal cycle of convective cloud produced by the monsoon trough has it's a pattern that is smoother than that produced by TCs.

It is noteworthy that a longer period of comparative storms can show a variation of precipitating clouds. In addition, raw radar reflectivity data provides more details of the precipitating clouds. Hence, expanded further detailed analysis using raw radar data should prove more revealing, and can be used to examine the physical process during the extreme events.

Acknowledgements

This research was supported by the National Research Council of Thailand (NRCT) through Naresuan University R2561B062 and R2562B031. We are deeply grateful to "Advancing Co-design of Integrated Strategies with Adaptation to Climate Change in Thailand (ADAP-T)" supported by the Science and Technology Research Partnership for Sustainable Development (SATREPS), JST-JICA for providing research funds to support the project. Special thanks to the Thai Meteorological Department and Hydro and Agro Informatics Institute for providing free downloadable radar reflectivity images. In addition, we gratefully thank the developer of the OpenCV and Wradlib libraries for providing source codes used in Python script to be adapted in the processing of radar reflectivity images.

References

Blackwell, K. G., 2000, Evolution of Hurricane Danny (1997) at landfall: Doppler-observed Eyewall Replacement, Vortex Contraction /Intensification and Low-Level Wind Maxima. *Monthly Weather Review*, Vol. 128, 4002-4016.

Fulton, R., Breidenbach, J., Seo, D. J., Miller, D. and O'Bannon, T., 1998, The WSR-88D Rainfall Algorithm. *Weather and Forecasting*, Vol. 13, 377-395.

Groisman, P. Y., Knight, R. W., Karl, T. R., Easterling, D. R., Sun, B. and Lawrimore, J. H., 2004, Contemporary Changes of the Hydrological Cycle Over the Contiguous United States: Trends Derived from in Situ Observations. *Journal of Hydrometeorology*, Vol. 5, 64-85, doi:10.1175/1525-7541(2004)-005<0064:CCOTHC>2.0.CO;2.

Heistermann, M., Jacobi, S. and Pfaff, T., 2013, Technical Note: An Open Source Library for Processing Weather Radar Data (Wradlib), *Hydrology and Earth System Sciences*, Vol. 17, 863-871.

Houze, Jr., R. A., 1989, Observed Structure of Mesoscale Convective Systems and Implications for Large-Scale Heating. *Quarterly Journal of the Royal Meteorological Society*, Vol. 115, 425-461.

Jorgensen, D. P., 1984, Mesoscale and Convective-Scale Characteristics of Mature Hurricanes. Part I: General Observations by Research Aircraft. *Journal of the Atmospheric Sciences*, Vol. 41, 1268-1285.

Kanae, S., Oki, T. and Musiake, K., 2011, Impact of Deforestation on Regional Precipitation Over the Indochina Peninsula. *Journal of Hydrometeorology*, Vol. 2, 51-70.

Kaplan, J. and DeMaria, M., 2001, On the Decay of Tropical Cyclone Winds after Landfall in the New England area. *Journal of Applied Meteorology*, Vol. 40, 280-286.

Karl, T. R. and Knight, R. W., 1998, Secular Trends of Precipitation amount, Frequency, and

Intensity in the United States. *Bulletin of the American Meteorological Society*, Vol. 79, 231-241, doi:10.1175/1520-0477(1998)079<0231-:STOPAF>2.0. CO;2.

Kessinger, C. Ellis, S. and Andel, J. V., 2003, The Radar Echo Classifier: A Fuzzy Logic Algorithm for the WSR-88D, 3rd Conf. on Artificial Intelligence Appl. To the Environ. Sci., American Meteorological Society.

Kucera, P. A. Krajewski, W. F. and Young, B. C., 2004, Radar Beam Occultation Studies Using GIS and DEM Technology: An Example Study of Guam. *Journal of Atmospheric and Oceanic Technology*, Vol. 21, 995-1006, doi:10.1175/1520-0426(2004)021<0995:RBO-SUG>2.0.CO;2.

Lang, T. J. Ahijevych, D. A. Nesbitt, S. W. and Carbone, R. E., 2007, Radar-Observed Characteristics of Precipitating Systems during NAME 2004. *Journal of Climate*, Vol. 20, 1713-1733.

Langston, C., Zhang, J., and Howard, K., 2007, Four-dimensional dynamic radar mosaic. Journal of Atmospheric and Oceanic Technology, Vol. 24, 776–790.

Lau, K. M. and Wu, H. T., 2007, Detecting Trends in Tropical Rainfall Characteristics, 1979-2003. *International Journal of Climatology*, Vol. 27, 979-988, doi:10.1002/joc.1454.

Lau, W. K. M., and Zhou, Y. P., 2012, Observed recent trends in tropical cyclone rainfall over the North Atlantic and the North Pacific. *Journal of Geophysical Research*, 117, D03104, doi:10.1029/2011JD016510.

Mahavik, N., Satomura, T. and Baimoung, S., 2013, Radar Rainfall Analysis in the Middle of Indochina Peninsula. *Journal of Disaster Research*, Vol. 8, 187-188.

Mahavik, N., Satomura, T., Shige, S., Sysouphanthavong, B., Phonevilay, S., Wakabayashi, M. and Baimoung, S., 2014, Rainfall Pattern over the Middle of Indochina Peninsula during 2009-2010 Summer Monsoon. *Hydrological Research Letters*, Vol. 8, 57-63.

Mahavik, N. and Tantanee, S., 2018a, The Convective Cloud Properties Extraction from Weather Radar Reflectivity during SONCA Tropical Storm over the Lower Northern Thailand. *Proceeding of Asian Conference on Remote Sensing 2018*, Vol. 3, 1604-1612.

Mahavik, N. and Tantanee, S., 2018b, Quality Assessment of Mosaicked Weather Radars over the Chao Phraya River Basin, Thailand. *Proceeding of GMSARN Int. Conf. on Energy, Environment and Development in GMS*, SD44, 1-4.

Mahavik, N. and Tantanee, S., 2019, Convective Systems Observed by Ground-Based Radar during the Seasonal March of Asian Summer Monsoons in the Middle of Thailand. *Engineering and Applied Science Research*, Vol. 46(4), 318-330.

Matsumoto, J., 1997, Seasonal Transition of Summer Rainy Season over Indochina and Adjacent Monsoon Region. *Advances in Atmospheric Sciences*, Vol. 14, 231–245, doi:10.1007/s00376-997-0022-0.

Matyas, C. J., 2010, Associations between the Size of Hurricane Rain Fields at Landfall and Their Surrounding Environments. *Meteorology and Atmospheric Physics*, Vol. 106, 135-148, doi: 10.1007/s00703-009-0056-1.

Matyas, C. J., 2013, Processes Influencing Rain-Field Growth and Decay after Tropical Cyclone Landfall in the United States. *Journal of Applied Meteorology and Climatology*, Vol. 52, 1085-1096, doi:10.1175/JAMC-D-12-0153.1.

McRoberts, D. B. and Nielsen-Gammon, J. W., 2017, Detecting Beam Blockage in Radar-Based Precipitation Estimates. *Journal of Atmospheric and Oceanic Technology*, Vol. 34(7), 1407-1422.

Medlin, J. M. Kimball, S. K. and Blackwell, K. G., 2007, Radar and Rain Gauge Analysis of the Extreme Rainfall during Hurricane Danny's (1997) Landfall. *Monthly Weather Review*, Vol. 135, 1869-1888.

Nesbitt, S. W. Cifelli, R. and Rutledge, S. A., 2006, Storm Morphology and Rainfall Characteristics of TRMM Precipitation Features. *Monthly Weather Review*, Vol. 134, 2702–2721.

Okumura, K. Satomura, T. Oki, T. and Warawut, K., 2003, Diurnal Variation Of Precipitation by Moving Mesoscale Systems: Radar Observations in Northern Thailand. *Geophysical Research Letters*, Vol. 30, doi:10.1029/ 2003GL018302.

Rabus, B. Eineder, M. Roth A. and Bamler, R., 2003, The Shuttle Radar Topography Mission-A New Class of Digital Elevation Models Acquired by Spaceborne Radar. *ISPRS Journal of Photogrammetry & Remote Sensing*, Vol. 57, 241-262.

Roy Bhowmik, S. K. Kotal, S. D. and Kalsi, S. R., 2005, An Empirical Model for Predicting the Decay of Tropical Cyclone Wind Speed after Landfall over the Indian Region. *Journal of Applied Meteorology and Climatology*, Vol. 44, 179-185.

Rinehart, R. E., 1999, Radar for meteorologists 3rd ed, Rinehart publication, P.O.Box6124, Grand Forks, ND 58206-6124, USA, 428.

Satomura, T., Katsumata, M., Mori, S., Yokoi, S., Matsumoto, J., Ogino, S. and Kamimera, Y., 2013, To Understand Typhoons' Behavior over Indochina. *Journal of Disaster Research*, Vol. 8, 153-154.

Satomura, T., Yamamoto, K., Sysouphanthavong, B. and Phonevilay, S., 2011, Diurnal Variation of Radar Echo Area in the Middle of Indochina. *Journal of the Meteorological Society of Japan*, Vol. 89a, 299-305, doi: 10.2151/jmsj.2011-A20.

Sugimoto, M. and Satomura, T., 2010, Long-lived typhoons over Indochina. *Journal of Engineering Science and Technology*, Vol. 7, 97-104.

Seo, D. J., Kondragunta, C. R., Kitzmiller, D., Howard, K., Zhang, J. and Vasiloff, S., 2005, The National Mosaic and Multisensor QPE (NMQ) Project—Status and Plans for a Community Testbed for High-Resolution Multisensor Quantitative Precipitation Estimation (QPE) over the United States. *Preprints, 19th Conf. on Hydrology, San Diego, CA, American Meteorological Society, 1.3.* [Available online at http://ams.confex.com-/ams/Annual2005/techprogram/paper_86485.htm.]

Steiner, M., Houze, R. A. and JR. Yuter, S. E., 1995, Climatological Characterization of Three-Dimensional Storm Structure from Operational Radar and Rain Gauge Data. *Journal of Applied Meteorology*, Vol. 34, 1978–2007.

Takahashi, H. G. and Yasunari, T., 2006, A Climatological Monsoon Break in Rainfall over Indochina-A Singularity in the Seasonal March of the Asian Summer Monsoon. *Journal of Climate*, Vol. 19, 1545-1556, doi:10.1175/-JCLI3724.1.

Takahashi, H.G. and Yasunari, T., 2008, Decreasing Trend in Rainfall over Indochina during the Late Summer Monsoon: Impact of Tropical Cyclones. *Journal of the Meteorological Society of Japan*, Vol. 86, 429-438, doi:10.2151/jmsj.86.429.

Takahashi, H. G., Yoshikane, T., Hara, M. and Yasunari, T., 2009, High-Resolution Regional Climate Simulations of the Long-Term Decrease in September Rainfall over Indochina. *Atmospheric Science Letters*, Vol. 10, 14-18, doi:10.1002/asl.203.

Takahashi, H. G., 2011, Long-Term Changes in Rainfall and Tropical Cyclone Activity over South and Southeast Asia. *Advances in Geosciences*, Vol. 30, 17-22, doi:10.5194/adgeo-30-17-2011.

Takahashi, H. G., Fujinami, H., Yasunari, T., Matsumoto, J. and Baimoung, S., 2015, Role of Tropical Cyclones along the Monsoon trough in the 2011 Thai Flood and Interannual Variability. *Journal of Climate*, Vol. 28, 1465-1476, doi:10.1175/jcli-d-14-00147.1.

Van Andel, J., 2001, Radar Echo Classifier Algorithm Development Using Python. Preprints, 30th International Conference on Radar Meteorology. *American Meteorological Society*, Munich, Germany, 19-24 July 2001, 704-707.

Vasiloff, S. V., and Coauthors, 2007, Improving QPE and very short term QPF: An initiative for a community-wide integrated approach. *Bulletin of the American Meteorological Society*, Vol 88, 1899–1911.

Xie, S. P., Xu, H. M., Saji, N. H. and Wang, Y., 2006, Role of Narrow Mountains in Large-Scale Organization of Asian Monsoon Convection. *Journal of Climate*, Vol. 19, 3420–3429, doi:10.1175/ JCLI3777.1.

Yokoyama, C. and Takayabu, Y. N., 2008, A Statistical Study on Rain Characteristics of Tropical Cyclones using TRMM Satellite Data. *Monthly Weather Review*, Vol. 136, 3848-3862.

Zhang, J., Howard, K. and Gourley, J. J., 2005: Constructing three-dimensional multiple radar reflectivity mosaics: Examples of convective storms and stratiform rain echoes. *Journal of Atmospheric and Oceanic Technology*, Vol. 22, 30–42.

Zhang, J., and Coauthors, 2011, National Mosaic and Multi-Sensor QPE (NMQ) System: Description, Results, and Future Plans. *Bulletin of the American Meteorological Society*, Vol. 92, 1321–1338, doi:10.1175/2011BAMS-D-11-00047.1.